JOURNAL OF AIRCRAFT
Vol. 31, No. 1, Jan.–Feb. 1994

Remote Sensing Observations of Winter Aircraft Icing Conditions: A Case Study

B. B. Stankov* and A. J. Bedard Jr.†
NOAA/ERL/Wave Propagation Laboratory, Boulder, Colorado 80303

This article describes how various combinations and arrays of remote sensors can be used to successfully predict aircraft icing conditions aloft. A case study, validated by pilot reports, is developed to illustrate the use of remote sensor data to predict aircraft icing conditions as well as verify icing forecasts. Surface-based remote sensing instruments and conventional instruments were used to study aircraft icing conditions during the winter storm of January 24–25, 1989, in the Denver, Colorado area. A unique combination of arrays of remote sensors was used to determine spatial and temporal distribution of supercooled liquid water. The remote sensors used were profiling radars, radio-acoustic sounding systems, multichannel microwave radiometers, and lidar ceilometers. Measurements used to predict aircraft icing conditions aloft included cloud liquid water, temperature profiles with high vertical (~150 m) and temporal (~15 min) resolutions, and the heights of cloud base, as well as estimates of cloud-top height with a temporal resolution of 15 min. Arrays of remote sensing instruments are shown to enhance detection and prediction of aircraft icing. Present and future remote sensing capabilities for detecting aircraft icing events are described. This icing case study is unique in combining arrays of remote sensors of various types to define the spatial and temporal distributions of supercooled liquid water, and in making comparisons with pilot reports as a means of verification.

I. Introduction

BECAUSE aircraft icing causes numerous operational problems and accidents, there is a need to improve predictions and verify forecasts. Westwater and Kropfli[1] recognized that data from existing NOAA Wave Propagation Laboratory (WPL) sensors could enhance the ability to predict aircraft icing conditions aloft. Specifically, these sensors could provide temporally continuous monitoring of supercooled liquid in clouds. This capability is not available from conventional measurements, which in the Denver, Colorado area consist of mesoscale surface observations of temperature, moisture, and winds from prototype regional observing and forecasting services (PROFS) mesonet as well as routine National Weather Service (NWS) surface and upper air network data. We present a case study of a winter icing storm that occurred on January 24–25, 1989, using data from a combination of remote and conventional sensors as an example of the usefulness of these techniques for aircraft operations to predict icing conditions, i.e., temperatures between −20°C and 0°C with moisture present. A range of meteorological conditions can contribute to hazardous icing conditions. These are summarized in Fig. 1. Commercial airline pilot reports (PIREPS) were used to define the occurrence and spatial distribution of aircraft icing conditions. Table 1 shows icing conditions described by PIREPS in the 64-km^2 area surrounding Denver. The icing conditions were light to moderate and lasted for 12 h, during which 10 different types of aircraft were affected. Remote sensing techniques were used to obtain wind profiles, temperature and humidity profiles, and physical parameters relating to clouds: liquid water content, water vapor content, and cloud-base height. Using these remote sensor measurements and the moist adiabatic approximation, we also inferred cloud-top height.

II. Background

Both icing and weather modification studies require a definition of spatial distribution of supercooled liquid water, which can be a difficult task. Hill[2] described methods to measure distributions of supercooled liquid water, including direct aircraft icing measurements and the addition of a vibrating wire sensor to rawinsonde humidity ducts. Since 1980,[3] radiometers have been used to make remote measurements of supercooled liquid water. For example, Deshler et al.[4] used a radiometer threshold of >0.1-mm integrated liquid water for 10 min to decide when to launch cloud-seeding aircraft. Reynolds[5] inferred supercooled liquid water distributions in clouds from observations of water-saturated layers using rawinsonde soundings, observations of rimed snowflakes at mountain observatories, aircraft platforms, and mountaintop icing-rate meters, as well as microwave radiometers.

Rauber and Grant,[6] in studies of cloud systems over the Park Range of the northern Colorado Rocky Mountains, found the preferred regions for supercooled liquid water in stratiform clouds were near cloud top, cloud base, and regions of

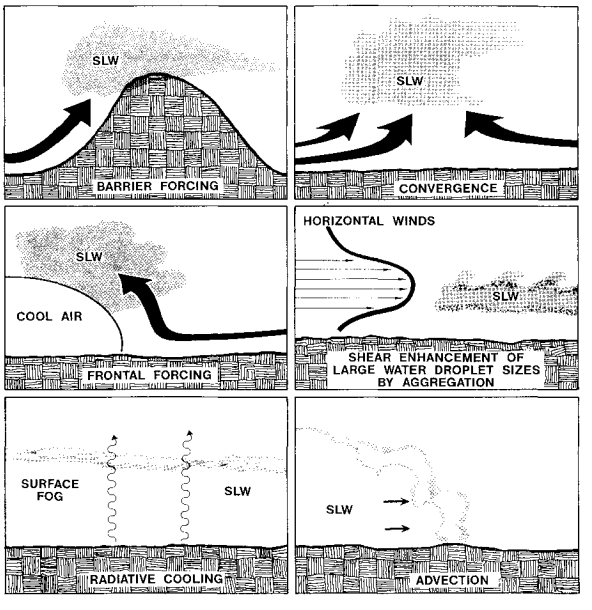

Fig. 1 Summary of atmospheric processes producing aircraft icing conditions.

Received Oct. 7, 1991; revision received Oct. 7, 1992; accepted for publication Oct. 13, 1992.

*325 Broadway. Member AIAA.
†325 Broadway. Senior Member AIAA.

orographic lifting. They found that near cloud top, small vertical velocities can sustain liquid water production because of the small size of ice crystals and slow associated growth rates in this region. Between cloud base and the −10°C level was another region of supercooled liquid water content, in part because of the distribution of ice crystals and in part because of high condensate supply rates near cloud base. The case study presented here shows a striking similarity to the results of Rauber and Grant,[6] suggesting that the mechanisms they identified can apply over a range of topographies and meteorological situations. Currently, icing forecasts are based on 12 hourly rawinsonde soundings and the NWS weather forecast.[7] Our article focuses on developing methods for combining remote sensor data and does not address cloud microphysics, which will be included in subsequent studies.

III. Parameters Measured by Remote Sensing Systems

To monitor aircraft icing conditions, it is necessary to establish whether liquid is present, where is it located, and if the air temperature is between 0 and −10°C, although icing occasionally occurs when it is as cold as −20°C. The remote sensors used in this case study were radiometers, a radio-acoustic sounding system (RASS), a wind profiler, and a lidar ceilometer; their capabilities and roles are described in Table 2.

Table 1 PIREP Icing levels and aircraft type on February 24–25, 1989

Time	Ice		Cloud		Aircraft
UTC	Intensity	Altitude, km AGL	Base, km AGL	Top, km AGL	Type
1615	1	2.13	1.74	2.04	B737
1630	1	2.07			BA46
1700	0			2.04	DA10
2130	1				MD80
2130	2	2.80			B727
2200	1	2.44			C550
2200	2	2.80		2.35	B727
2215	1	2.44			ALL
2230	1	2.44			C550
2330	1	2.44		2.59	MU2
0000	2	2.29		2.59	C550
0015	1	2.29		2.44	C414
0030	1			2.59	MU2
0030	2			2.44	C550
0030	3	1.98			BE20
0200	2				CR35
0400	1				BE02
0545	3	1.83			B737
0615	3	1.83			B737

Note: No SIGMET (significant weather warning) issued; ice intensity below severe.

A. Temperature and Water Vapor Profiles

To obtain continuous temperature and water vapor profiles, we used a six-channel microwave radiometer at Stapleton International Airport in Denver.[8] The radiometer measures emissions from six frequency bands: the 20.6-GHz water vapor channel, the 31.65-GHz liquid water channel, and four frequencies in the 50–60-GHz oxygen band for temperature measurements. These six brightness temperature measurements together with surface temperature, humidity, and pressure are used in a statistical inversion technique[9] that provides smooth vertical profiles of temperature and humidity up to about 300 mb every 2 min. From these profiles, geopotential heights and integrated water vapor can be derived with accuracies comparable to those of radiosondes. However, radiometrically determined profiles lack the vertical resolution (150 m) necessary to detect the elevated temperature inversions often associated with surface fronts.

RASS uses combined acoustic and radar techniques to measure virtual temperature profiles.[10,11] In this study we used the Stapleton RASS, which operates at a radio frequency of 915 MHz and an acoustic frequency of 2 kHz. This system obtains profiles every 15 min in the lowest 1.5 km, has a high vertical resolution of ~150 m, and thus has the ability to measure the structure of elevated inversions.[12] The RASS operated for 6 h during the period of strongest aircraft icing reported.

B. Wind Profiles

A 915-MHz wind-profiling radar at Stapleton[13,14] provided vertical profiles of the horizontal wind every 15 min. This provided independent information on the cloud's possible vertical extent by defining regions of shear and mixing. Those regions also provide conditions for large drop formation, and large drops accrete to an aircraft body very well. For the present study, the vertical wind component was not measured; current computer limitations at the profiler site prohibit simultaneous measurements of RASS virtual temperature and vertical wind.

C. Cloud-Related Quantities

The 20.6- and 31.65-GHz bands of the six-channel radiometer at Stapleton provided measurements of the vertically integrated liquid water and water vapor. A two-channel microwave radiometer[8] located ~50-km north of Stapleton, at Platteville, Colorado, measured the vertically integrated water vapor and liquid at that site. We also used the new-generation NWS lidar ceilometer[15] to measure cloud-base height at Stapleton.

Table 2 Summary of remote sensors used

Sensor	Measurement capabilities	Role	Location
Radiometers			Stapleton airport
Six-channel	Continuous temperature and humidity profiles	Provide temporal trend information about temperature Identify cloud liquid and monitor vapor	
Two-channel	Integrated liquid water Integrated water vapor	Identify cloud liquid and monitor vapor	Platteville
RASS	Continuous temperature profiles with high resolution in the vertical	Indicate regions in which supercooled liquid could exist	Stapleton airport
Wind profilers	Continuous horizontal and vertical wind profiles	Provide independent estimate of cloud-top height; integral part of Richardson number calculation	Stapleton airport
Lidar ceilometers	Continuous cloud-base height	Provide information on liquid water location	Stapleton airport

Table 3 Remote sensor characteristics

Sensor	Accuracy	Height resolution	Altitude range
Radiometers			
Six-channel	2°C	Details smoothed	0.0–30.0 km
Two-channel[a]			
Liquid	2.0 mm	Integrated value	
Vapor	0.8 mm	Integrated value	
RASS			
915 MHz	0.6°C rms estimate	150 m	0.2–1.5 km
Wind profiler			
915 MHz	1.5 m s^{-1}	150 m	0.2–6.0 km
Lidar ceilometers	60 m	30 m	0.03–3.5 km

[a]Rain below cloud base can be a source of error.

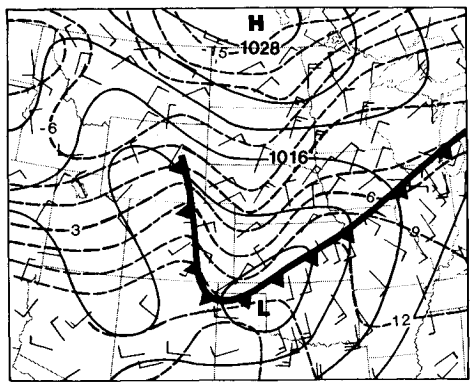

Fig. 2 Analysis of surface atmospheric observations (SAO) data at 0000 UTC 24 January. Temperature in °C (dashed lines), pressure in mb (solid lines). Wind flag = 25 m s^{-1}, barb = 5 m s^{-1}, half barb = 2.5 m s^{-1}.

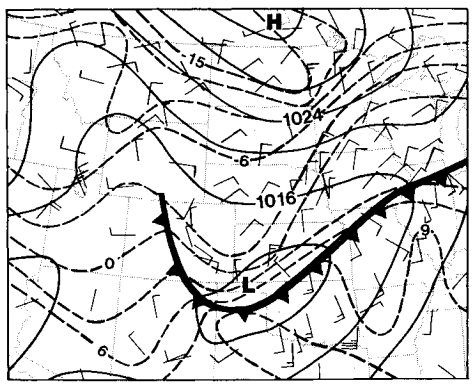

Fig. 3 Analysis of surface atmospheric observations (SAO) data at 0500 UTC 24 January. Temperature in °C (dashed lines), pressure in mb (solid lines). Wind flag = 25 m s^{-1}, barb = 5 m s^{-1}, half barb = 2.5 m s^{-1}.

IV. Remote Sensor Characteristics

Table 3 summarizes characteristics of the key remote sensors used in this study, based on findings in the following references. Hogg et al.[8] discuss the accuracy of radiometer measurements of water vapor and show them to be equivalent to the values obtained by integrating rawinsonde humidity profile measurements. Radiometer-retrieved temperature accuracies are reviewed by Hogg et al.[14] May et al.[11] compared RASS temperature profiles with rawinsonde measurements and showed that under conditions of light winds, similar to our situation, differences were within 0.6°C. Strauch et al.[16] summarize the characteristics of wind profilers, indicating their value for a range of uses in support of flight operations. Ceilometer characteristics are given by Vaisala.[17]

V. Meteorological Overview

The meteorological conditions between 0000 UTC 24 January and 0800 UTC 25 January 1989 were typical of shallow, anticyclonic winter storms up the slopes of the high plains that lead to the front range of the Rocky Mountains.[18–20] The storm produced no precipitation, but it did cause aircraft icing, as reported in PIREPS.

A. 0000 UTC 24 January 1989

At 0000 UTC 24 January, a surface cold front, leading a shallow, continental polar air outbreak, was situated over eastern Colorado (Fig. 2). Although the surface wind in Denver had already switched to northeasterly, the temperature drop associated with frontal passage had not yet occurred. The temperature in the Denver area was 9°C, and the dewpoint depression was 17°C. The eastern side of the cold front,

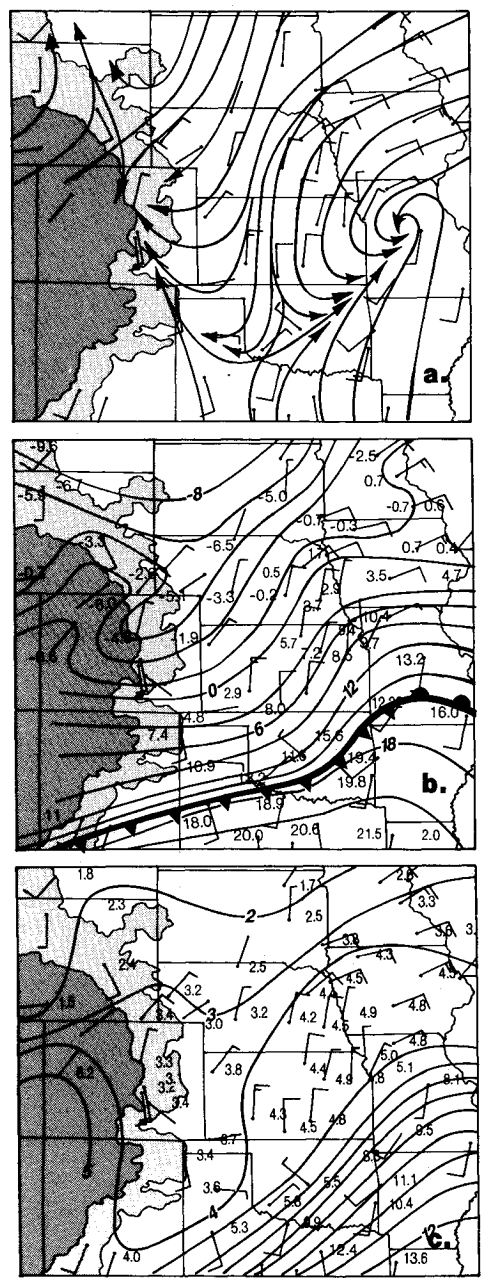

Fig. 4 Surface analysis of data averaged for 6 h between 1900 UTC 24 January and 0100 UTC 25 January: a) streamlines, b) temperature in °C, and c) absolute humidity in g m^{-3}.

unobstructed by the mountains, had already reached the southern borders of Colorado and Kansas, bringing relatively moist air to the eastern part of Colorado.

B. 0500 UTC 24 January 1989—First Cold Air Surge

The surface cold front passed through the Denver area at 0500 UTC 24 January, followed by northeasterly winds (Fig. 3). The Denver temperature dropped to −3°C, and the dewpoint depression decreased to below 1°C. Influenced by the Rocky Mountains, frontal progression southward accelerated. By 1100 UTC, a secondary surface low had developed at the Utah-Wyoming border. In response, the Denver wind became southerly and the temperature rose slightly.

C. 1700 UTC 24 January 1989—Second Cold Air Surge

At 1700 UTC 24 January, the shallow surge of cold air continued farther south, and by 0000 UTC 25 January, it extended over New Mexico and the Oklahoma-Texas border. Behind the cold front, the surface anticyclone intensified to 1038 mb.

Figure 4 shows a 6-h average surface data analysis of the wind, temperature, and absolute humidity for the period between 1900 UTC 24 January and 0100 UTC 25 January, during the second cold air surge and the occurrence of aircraft icing. The streamlines on Fig. 4a show the flow over Colorado from the northeast near the surface. This indicates that the low-level moisture in the Denver area was transported from the high plains and condensed when the vertical motion was enhanced by the front range slope. Because the air temperatures were low (~ −5°C) and the dewpoint temperature was near saturation (~ −5.6°C), strong vertical air motions were not necessary to cause stratus cloud formation. The cloud's western edge was blocked from spreading upward by the frontal inversion at about 900 m above ground level (AGL) [ground level is 1.611-km mean sea level (MSL) at Stapleton]. Figure 5a shows the streamlines and the temperature at the 500 mb surface, and Fig. 5b shows the absolute humidity at the same surface. The flow is dry, southerly, and not very cold. Figure 6 shows the situation schematically.

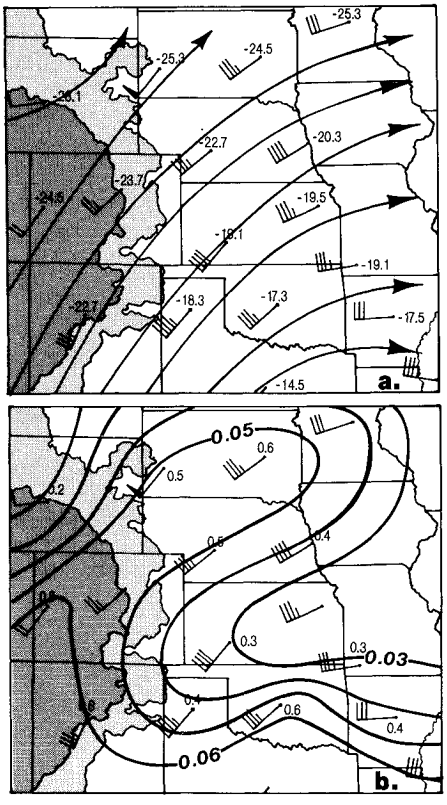

Fig. 5 500-mb pressure height data analysis for 0000 UTC 25 January: a) streamlines and temperature in °C at each station and b) absolute humidity in g m^{-3}.

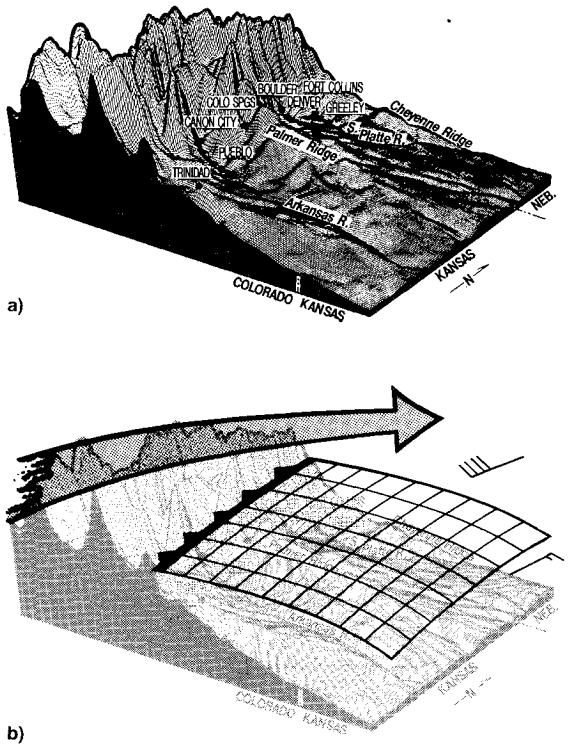

Fig. 6 a) Relief map of the high plains and the front range in Colorado. The terrain is exaggerated 50 times in the vertical to show the slope. b) Schematic model of upslope anticyclonic storm. Within the frontal inversion stratus forms because of the upslope motion over the high plains.

VI. Evolution of Vertical Profiles of Wind and Temperature

As discussed in Sec. III.B., vertical profiles of the horizontal wind are useful as an independent estimate of the existence of the shear layers and enhanced mixing above the stratus cloud layer. Mixing produces regions with large drop size as well as limits the vertical extent of the cloud. The 915-MHz wind profiler at Stapleton provided wind velocity profiles every 15 min. We used the PROFS Mesonet surface data from Aurora, Colorado to linearly interpolate the wind velocity between the ground (1.611-km MSL) and the first level of the wind profiler at 200-m AGL (1.811-km MSL). In addition, we identified and removed questionable measurements by filtering the data using the technique described by Velleman and Hoaglin.[21] This exploratory data analysis technique uses nonlinear median filters to remove outlying data points. Figure 7a shows every third filtered and interpolated wind profile for the 32 h between 0000 UTC 24 January and 0800 UTC 25 January. The wind shifted to northerly at 0000 UTC on January 24 and remained northerly for 13 h. A period of southerly flow at the 800-mb level occurred between 1100 and 1600 UTC on 24 January, and the flow reached the surface at 1200–1300 UTC. This southerly flow was associated with the formation of a secondary low-pressure center at the Utah-Wyoming border. At 1400 UTC, a new surge of northerly air, associated with the onset of upslope clouds, began to move through the Stapleton area. The shear zone associated with the new surge increased in height during the 17-h period that followed, and was a factor in limiting the vertical extent of the clouds. Figure 7b represents the time-height contour analysis of the N-S wind velocity. In this case, the zero line clearly marks northerly flow near the ground and southerly flow aloft. Throughout the 32-h period, the wind remained weak, and

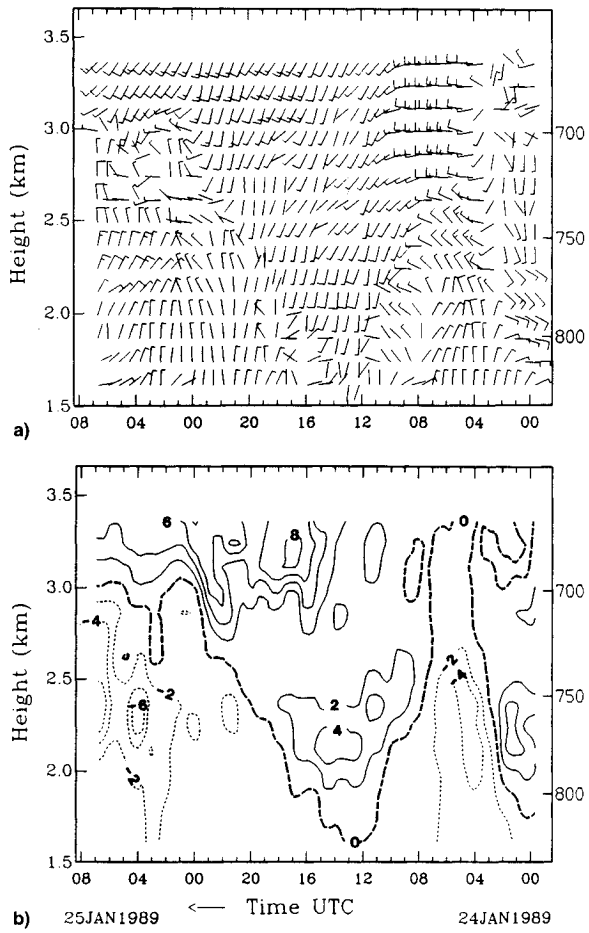

Fig. 7 a) Wind velocity 15-min profiles measured by the 915-MHz Stapleton wind profiler between 0000 UTC 24 January and 0800 UTC 25 January. Wind flag = 25 m s^{-1}, barb = 5 m s^{-1}, half barb = 2.5 m s^{-1}. b) Time-height analysis of N-S component of wind velocity *V*. Thin dashed lines are negative (northerly), thin solid lines are positive (southerly), and thick dashed line is zero. Ground level is at 1.611 km.

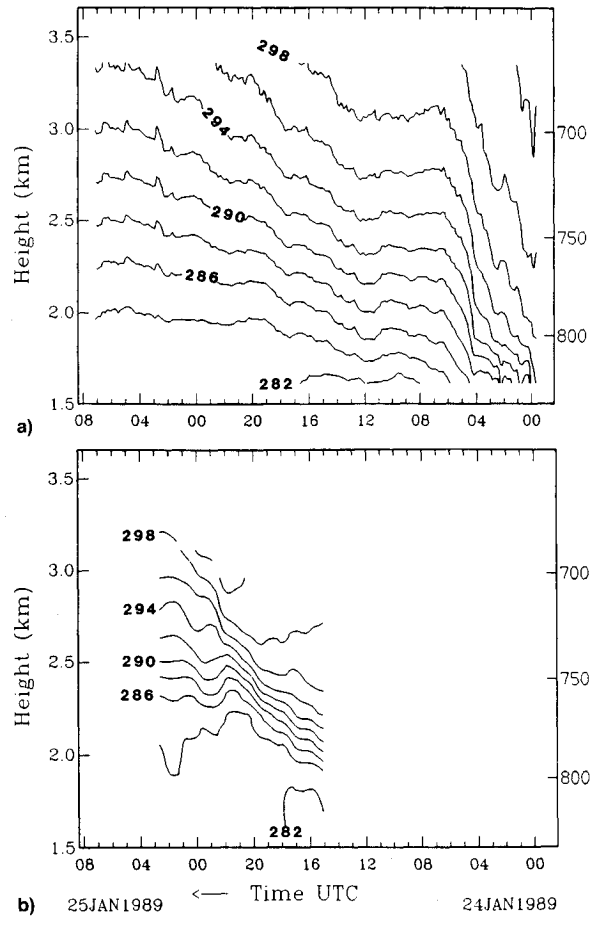

Fig. 8 a) Time-height analysis of θ (K), measured by the Stapleton six-channel microwave radiometer and b) time-height analysis of θ (K), measured by the Stapleton RASS, between 0000 UTC 24 January and 0800 UTC 25 January. Ground level is at 1.611 km.

the strongest wind speeds within the cold air reached ~7 m s^{-1}. Wind speeds inside the warm air above were not much stronger, and the transport of the cold air southward was quite slow.

The six-channel microwave radiometer provided a temperature profile every 2 min. These temperature profiles permitted construction of the time-height potential temperature (θ) analysis shown in Fig. 8a. The first surge of cold air occurred in the evening hours (~0000 UTC) and encountered the stable boundary layer already cooled by nocturnal radiation. Because of this, the potential temperature drop at the surface was not very pronounced. However, at 0.5-km AGL (2.111-km MSL) the potential temperature dropped by 4 K in 1.5 h. Because of the poor vertical resolution of the microwave radiometer, the second cold air surge is not evident in Fig. 8a. The inversion strength remains the same after the initial cold air surge. On the other hand, the RASS potential temperature (θ) analysis in Fig. 8b shows the second cold air surge very dramatically. This is possible because of the high vertical and temporal resolution of the RASS measurements. Between 1900 and 2100 UTC, the potential temperature isolines are packed tightly, showing the increase in inversion strength caused by the transport of cooler air beneath the inversion.

Stapleton rawinsonde profiles of temperature and dewpoint temperature for 2300 UTC 24 January are shown in Fig. 9, together with the radiometer profiles of temperature and dewpoint temperature and the RASS temperature profile. The rawinsonde measured an inversion of 2.6°C, the radiometer an isothermal layer 100–900-m AGL (1.711–2.511-km MSL), and the RASS profile an inversion of 5°C. The rawinsonde profiles in this figure indicate near-saturated air in the lowest 700-m AGL; the radiometer profiles indicate a saturated layer between 100–700-m AGL (1.711–2.311-km MSL). Because of the poor vertical resolution of the microwave radiometers, the radiometer-retrieved profiles of temperature and dewpoint temperature can be expected to miss elevated inversions. Schroeder et al.[22] discuss this problem and suggest a method of combining satellite observations, radiometer measurements, and RASS measurements to obtain a better representation of the elevated inversions. All three profiles indicate that if liquid water were found beneath the inversion, it would be supercooled. The RASS profile showed the warmest temperatures at the cloud base and the cloud top, thereby indicating more potential for large supercooled droplet formation[23,24] in those regions.

Figure 10a shows the stacked hourly temperature profiles during the second surge of cold air. The strongest inversion, of ~10°C, occurred at 1900 UTC 24 January during the second cold air surge. The radiometer measurements do not show this inversion at all, and the rawinsonde data were not available at this time. Figure 10b shows the time-height analysis of the RASS-measured temperatures for the period in Fig. 10a. The RASS data, because of their high vertical and temporal resolution, were able to show a temperature drop beneath the inversion that could cause liquid water to become supercooled. This is clear evidence of the value of observing the aircraft icing events with high vertical and temporal resolution remote sensing instruments as well as conventional instruments.

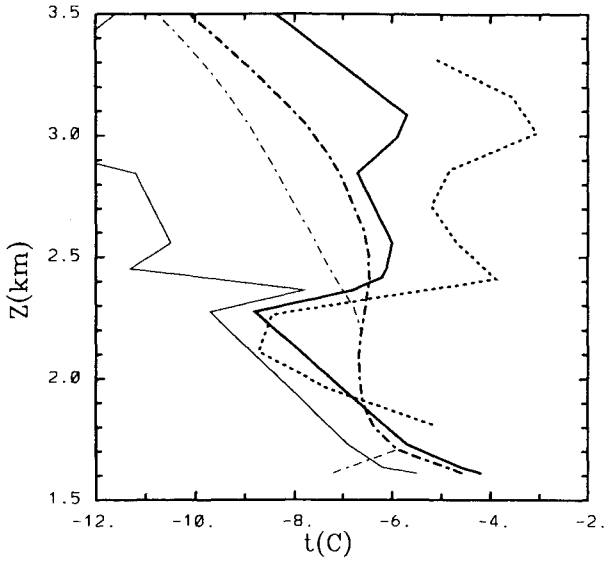

Fig. 9 Profiles taken at 2300 UTC 24 January of temperature (bold lines) and dewpoint temperature (thin lines) in °C by Stapleton rawinsonde (solid lines), Stapleton microwave radiometer (dashed-dotted line), and Stapleton RASS (dotted line). Ground is level at 1.611 km.

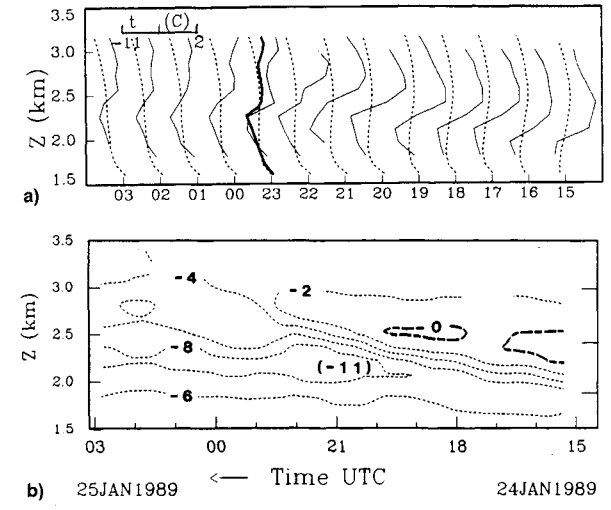

Fig. 10 a) Stacked hourly temperature profiles measured by the Stapleton RASS (thin solid lines), by the Stapleton rawinsonde (bold solid line), and by microwave radiometer at Stapleton (dotted lines), between 1500 UTC 24 January and 0300 UTC 25 January. Temperature is in °C; minimum is −11°C and maximum is 2°C. b) Time-height analysis of RASS temperature in °C, for the same period as in a). Ground level is at 1.611 km.

VII. Spatial and Temporal Distribution of Liquid and Water Vapor

When some path-integrated liquid water exists, and the air temperature is between −20 and 0°C, an aircraft icing hazard is present. Moreover, the hazard increases with the amount of liquid. Time series of liquid water measurements from the six-channel, zenith-pointing, microwave radiometer at Stapleton are shown in Fig. 11b. The vertically integrated liquid amount remained zero from 0000 to 1000 UTC on 24 January. The first passage of the cold front through the Denver area did not produce any liquid water. At 1000 UTC, liquid water amount increased, and it reached 0.15 mm at 1730 UTC. This was the time of the secondary low-pressure formation at the Utah-Wyoming border and of southerly winds in the Denver area. The maximum of 0.35 mm in vertically integrated liquid was reached at 0410 UTC 25 January. This increase was associated with the second cold air surge through the Denver

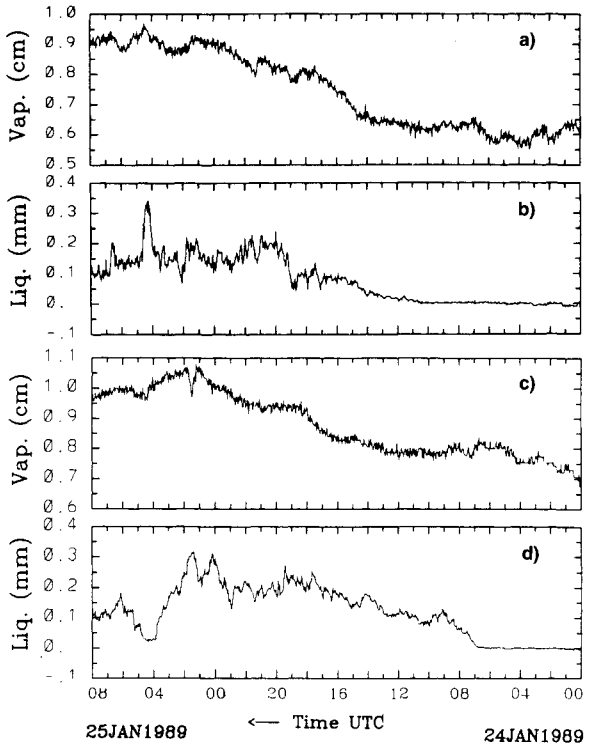

Fig. 11 Time series of a) water vapor and b) liquid water measured by Stapleton six-channel microwave radiometer; time series of c) water vapor and d) liquid water measured by Platteville two-channel microwave radiometer between 0000 UTC 24 January and 0800 UTC 25 January.

area. The RASS data showed that the temperature at 0.5-km AGL (2.111-km MSL) dropped to −11°C at 1900 UTC. This provided conditions for supercooled liquid water formation, which are described by Decker et al.[25] and Politovich.[23] After 1900 UTC, the liquid amount dropped to 0.15 mm. The total water vapor measurements show a similar trend (Fig. 11a). The water vapor started increasing with the second surge of the cold, moist air after the period of southerly winds at Stapleton and reached a maximum of 0.95 cm at 0415 UTC. Figure 11d shows the time series of the vertically integrated liquid water amount measurements from the two-channel, zenith-pointing, microwave radiometer at Platteville, and Fig. 11c shows the total water vapor measurements from the same radiometer. The liquid amount at this site shows a much sharper and earlier increase; it reached 0.15 mm at 1300 UTC 24 January and 0.35 mm at 0130 UTC 25 January. Indeed, since Platteville is located about 50-km north of Denver and the cold air is moving at about 5-m s^{-1}, it should take ~3 h to travel this distance. This observation emphasizes the potential of arrays of radiometers for tracking advecting systems.

Satellite and radiosonde observations indicate the presence of another cloud deck above, at the ~500-mb level, which prevented us from making estimates of the cloud-top height of the lower deck.

Figure 12 shows the surface absolute humidity, temperature, and potential temperature distributions in the Mesonet area. The cold, moist air flow from the northeast is trapped by the Rocky Mountains to the west and Palmer Ridge to the south [indicated by the Mesonet station Elbert (ELB)].

VIII. Pilot Reports

Although our data from remote sensors showed a clear potential for monitoring aircraft icing conditions, aircraft verification was required. In the absence of research aircraft data, we searched through the available PIREPS data. Figure 13a shows icing PIREPS locations inside the Mesonet area. Most of the reports are for the Stapleton Airport area, but there

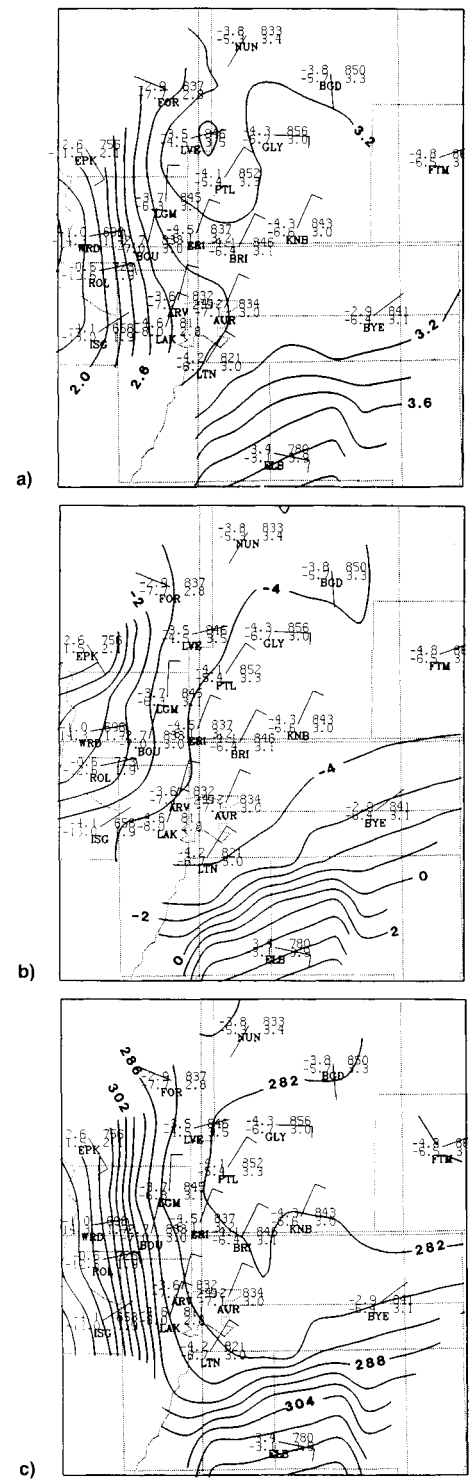

Fig. 12 Mesonet data analysis of a) surface absolute humidity in g m^{-3}, b) surface temperature in °C, and c) surface potential temperature in K at 1900 UTC 24 January. The four numbers around each station are temperature (top left) in °C, dewpoint temperature (bottom left) in °C, surface pressure (top right) in mb, and absolute humidity (bottom right) in g m^{-3}.

are reports of light icing north of the Cheyenne Ridge at 500–1000-m AGL (2111–2611-m MSL) and of moderate icing around Platteville below 2111-m MSL. Figure 13b is an expanded view of the area around Stapleton Airport; PIREPS show icing of light-to-moderate intensity mostly at 500–1000-m AGL (2111–2611-m MSL). However, according to one report, moderate icing below 500-m AGL (2111-m MSL) occurred at 0000 UTC on 25 January.

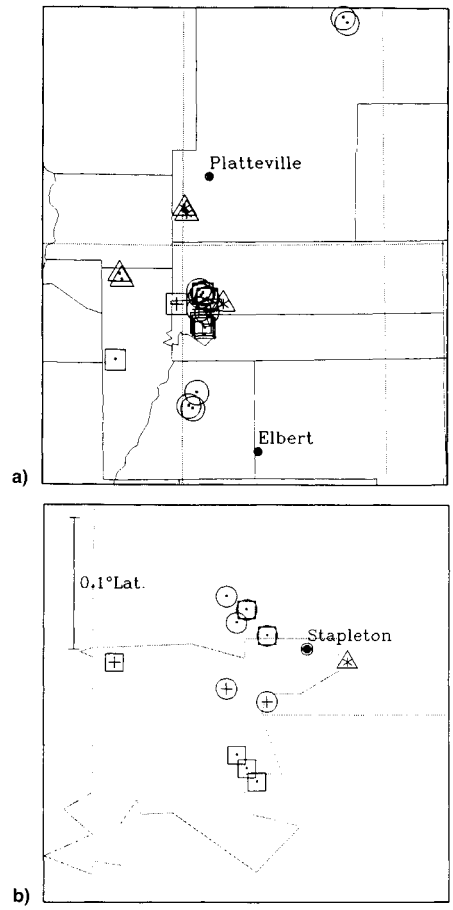

Fig. 13 a) Analysis of PIREP data inside the Mesonet area, concerning aircraft icing from 0000 UTC 24 January to 0800 UTC 25 January, and b) enlargement of the Denver area counties. △ below 500 m, ○ 500–1000 m, and □ above 1000 m; ● = light, + = light-to-moderate, and ∗ = moderate.

Pilot reports of icing are a valuable component of systems designed to avoid dangerous aircraft icing conditions, especially when combined with remote sensing information that can define the flight environment quantitatively. Moreover, arrays of combined remote sensors can identify the icing hazard potential of advecting boundaries before their arrival at some critical region. For example, in this case study, the liquid water increased at Platteville approximately 3 h before the increase was observed at the airport. Nevertheless, pilot reports provide confirmation of the existence of a hazard, and the following sections compare pilot reports with remote sensor reconstruction of atmospheric fields.

IX. Method for Estimating Cloud-Top Height from Surface Remote Sensor Measurements

The height of cloud base measured by the Stapleton ceilometer every 30 s is presented in Fig. 14a. Cloud onset was at 1000 UTC 24 January, and the cloud-base height fluctuated between 100–400-m AGL (1.711- and 2.011-km MSL) for the next 22 h. Figure 14b shows the estimated height of the cloud top; the method described by Cox et al.[26] for cloud-depth computation was extended to obtain this estimate. The following steps describe our computation of the cloud top estimate.

A. Step 1: Obtain Cloud Depth

1) Assume moist adiabatic approximation inside the cloud, 2) assume the liquid water and water vapor are mixed inside the cloud layer, and 3) assume the liquid water content (g kg^{-1}) is a linear function of height.

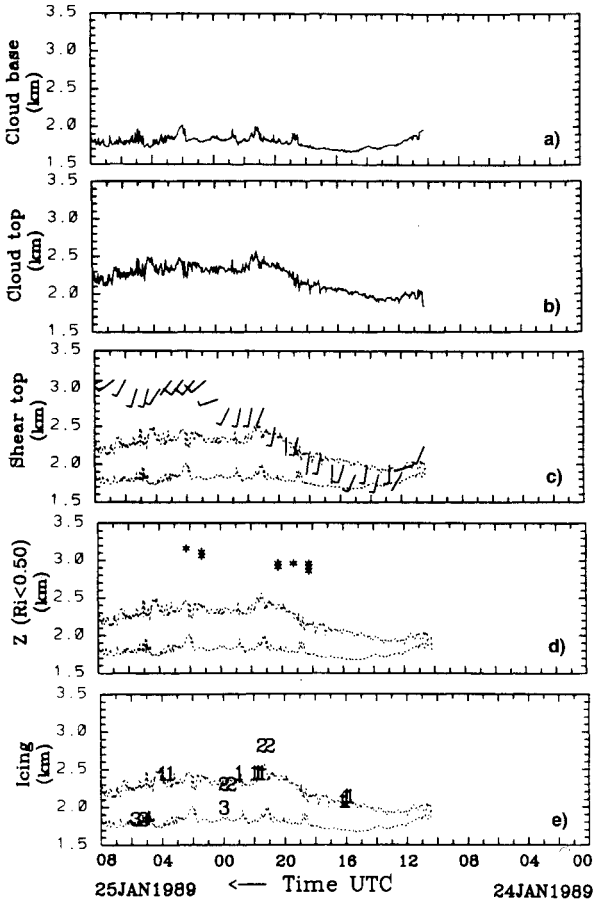

Fig. 14 a) Cloud-base height measured by Stapleton ceilometer; b) cloud top computed using moist adiabatic relation and the measurement of liquid water and cloud-base height; c) wind barbs at the top of the shear zone between the northerlies near the ground and the southerlies aloft (wind flag = 25 m s^{-1}, barb = 5 m s^{-1}, half barb = 2.5 m s^{-1}) obtained from wind profiler data; d) height where the Richardson number computed using RASS and wind profiler data is ≤0.5; and e) aircraft icing height from PIREP, where 1 = light, 2 = light-to-moderate, and 3 = moderate. In Figs. 14c–e cloud-base height and cloud-top height from Figs. 14a and 14b are repeated in dashed line. Ground level is at 1.611 km.

B. Step 2: Obtain Cloud-Top Height

1) Apply ceilometer measurements of cloud-base height, and 2) apply microwave radiometer measurement of path integrated liquid water.

Although moist adiabatic conditions are never truly reached in winter storms over the continent, the computed cloud-top height is in good agreement with the inversion top of Fig. 8. The computed cloud-top height time series fluctuates between 300–900-m AGL (1.911- and 2.511-km MSL). Because the air displaced by the second cold air surge was also relatively moist, the cloud may have extended a short distance above the inversion. Figure 14c shows the wind barbs at the top of the shear zone, and the cloud-base and cloud-top heights of Figs. 14a and 14b are repeated. Figure 14d shows the time and height where the Richardson number, computed from the RASS and wind profiler data, is less than 0.5, and the cloud-base height and cloud-top height time series. Two points at 2000 UTC 24 January represent the heights where the Richardson number was less than the critical value of 0.25. This is a strong indication of shear layer instability, and therefore, of mixing above the cloud-top height obtained from the moist adiabatic approximation. Figure 14e shows the aircraft icing PIREPS of Fig. 13, and the cloud-base height and cloud-top height time series. Most of the light icing occurred at the top of the cloud; however, there were three reports of moderate icing below 400-m AGL (2011-m MSL). Rauber and Grant[6] and Reynolds[5] describe a conceptual model of the orographic cloud with the preferred locations of supercooled liquid water zones inside it. PIREPS locations in Fig. 14e show remarkable similarity to their conceptual models. The icing occurred after the second surge of the cold air through the Stapleton area. The two light-to-moderate aircraft icing PIREPS above the computed cloud-top height can be explained either by the commercial pilots not reporting the exact level of icing occurrence or by the cloud-top height computation giving only the minimum cloud depth; however, both do agree very well with the height of the shear zone between the northerly flow near the ground and the southerly flow aloft. Indeed, the mixing above the cloud-top height determined from the moist adiabatic approximation might have caused the cloud to extend higher.

The fact that in this case upper-level cloud cover prevented the use of satellite information to obtain the cloud-top temperature of the lower cloud layer, and hence, to infer cloud-top height, emphasizes the need for combining a range of remote sensor information. In an analysis of forecasts of supercooled liquid water distribution, Flueck and Reynolds[27] indicate that satellite data are the most heavily relied on for forecasting, and limited finemesh model (LFM) output and radiometer data are used to a lesser extent. For situations similar to our case study, which occur frequently along the front range of Colorado, satellite data often will not be useful.

X. Applications of Richardson Number Profiles Obtained from Remote Sensor Measurements

Gossard et al.[28] describe the use of a ground-based Doppler radar for detecting precipitation and melting level. Although information concerning the drop-size distribution is obtained, this is primarily for drop sizes greater than 200 μm with high terminal velocities, which are probably not a factor in icing events. Politovich[23,24] has shown that drops in the intermediate range from 20 to 200 μm can produce rapid formation of ice on aircraft surfaces. The importance of drops in this size range has been verified in laboratory experiments.[29] However, a valuable application of the Doppler radar techniques of Gossard et al.[28] is to identify regions of precipitation that could make the interpretation of radiometer data more difficult. Liquid water falling below cloud base causes errors in estimates in those locations of the amount of supercooled liquid water, since the radiometer senses all the integrated liquid above the sensor.

An additional factor is the presence of liquid water on exposed radiometer reflector surfaces. This could happen from melting snow or rain. Stankov et al.[30] discuss methods for keeping these surfaces free of liquid water. These problems have also been identified by Heggli and Rauber.[31]

We also applied Doppler radar in conjunction with RASS to identify regions of low Richardson number. Regions of low Richardson number have been associated with aircraft turbulence,[32] and a recent study by Pobanz and Marwitz[33] found

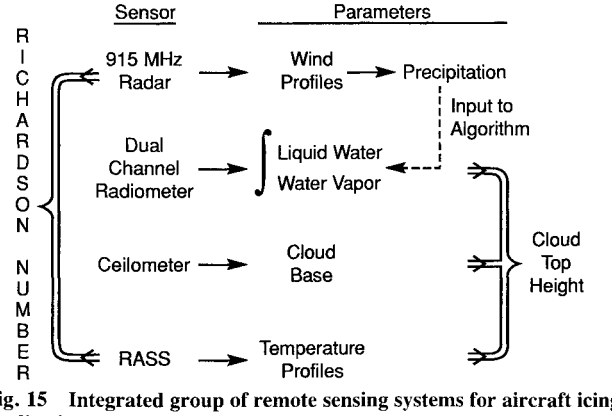

Fig. 15 Integrated group of remote sensing systems for aircraft icing applications.

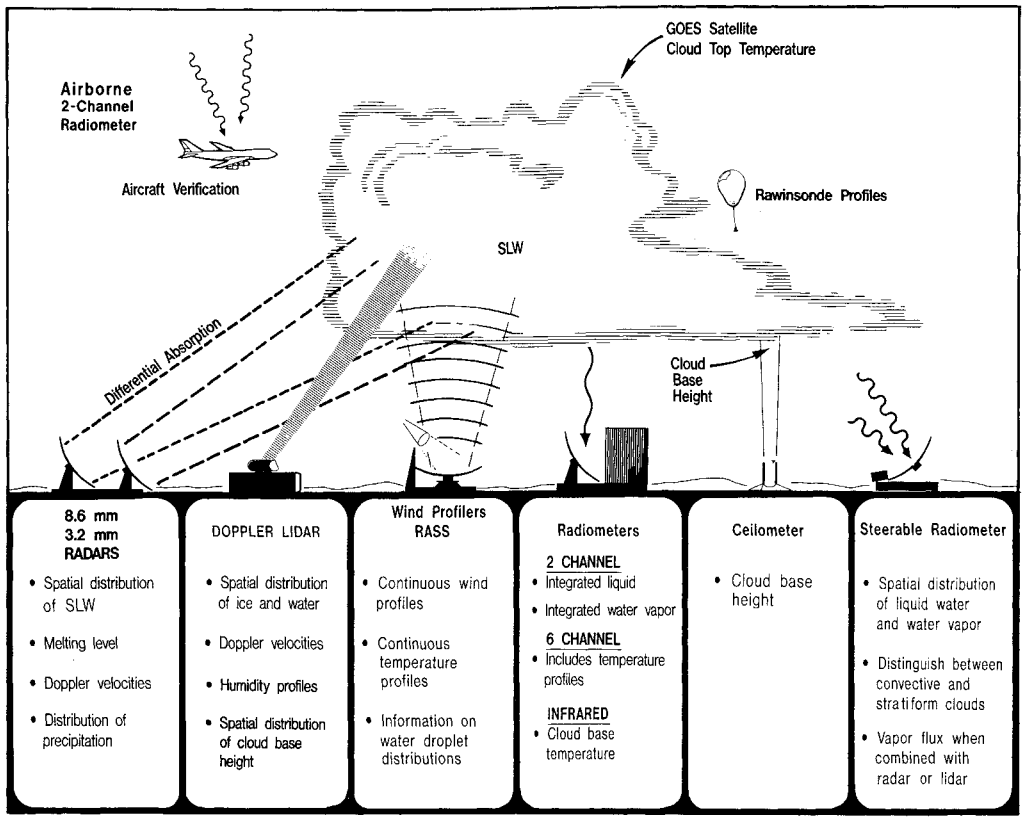

Fig. 16 Combined capabilities of wave propagation laboratory remote sensing instruments for measuring supercooled liquid water.

a correlation between regions of small Richardson number and regions with larger drop sizes of supercooled liquid water. This is consistent with the predictions of Reuter et al.[34] as well as those of Baker et al.[35] In addition, measurements of wind and temperature profiles can be used to infer cloud-top heights and should apply to meteorological situations similar to those described here. Thus, profiles of Richardson number can be valuable for several reasons, including the identification of regions of larger drops of supercooled liquid water and of increased probability of aircraft icing.

XI. Implications for the Design of an Integrated System of Remote Sensors for Aircraft Icing Studies

The capabilities provided by various sensors can be enhanced by their combined use and suggest the configuration outlined here. Past investigators have applied some of these combinations, but recent improvements in RASS, as well as in signal processing techniques, make the integrated group of sensors suggested here feasible.

Examples of past work on combined sensors summarized below emphasize that many investigators explored the potential of combined sensors to obtain needed information on the spatial distribution and microphysics of supercooled liquid water. In particular, Heggli and Reynolds[36] combined a K-band radar and dual-channel radiometer in an experiment to identify cloud characteristics associated with integrated liquid water. They also recommended that arrays of radiometers be applied to define spatial distributions. Popa Fotino et al.[37] suggested the use of scanning radiometers and a network of observing sites. Rauber and Grant[38] applied a K-band radar, a dual-channel radiometer, and a C-band surveillance radar. Sassen et al.[39] included a polarization radar with this ensemble of instruments, also noting the potential value of real-time availability of these data. Figure 15 illustrates a grouping of sensors that can provide information on an array of parameters important for icing forecast verification, including computation of cloud-top height and Richardson number. In addition, one sensor (e.g., Doppler radar) can be valuable for insuring a reasonable interpretation of another (e.g., a dual-channel radiometer), in this case by providing information on precipitation.

We believe that such a combined system would be cost effective at or near aircraft terminals and could also provide information to help reduce other important hazards in addition to aircraft icing. We envision that real-time displays of radiometer time series would be displayed on forecaster work stations along with profiles of wind and temperature. Computed quantities such as cloud-top height and Richardson number would also be displayed. Such a resource should enable forecasters to assess icing potential and location and predict advecting fields. Other aviation applications include evaluating microburst potential using boundary-layer lapse rate measurements[40] and predicting wake vortex positions.[41]

XII. Summary

This case documenting icing in the January 24–25, 1989 storm illustrates the importance of remote sensing as well as conventional observations in detecting conditions that can cause aircraft icing. The most important capabilities demonstrated for the Stapleton International Airport area are the following:

1) Continuous measurements of the vertically integrated liquid water with microwave radiometers were used to determine cloud liquid water.

2) Continuous RASS temperature profiles (having high vertical and temporal resolution) defined the temperature drop sufficient for supercooled liquid water formation (Fig. 10 shows this dramatically).

3) Continuous measurement of cloud-base height and computation of cloud-top height indicated the vertical location of supercooled liquid water.

4) Continuous measurements of wind profiles permitted the location of shear zones, providing more complete specification of icing events.

Figure 16 summarizes the techniques now available at WPL that can be applied to the aircraft icing problem. Most ob-

servations described can be made routinely with unattended instruments, but some of the newer techniques require skilled operators.

We realize that numbers of cases need to be studied before confidence can be obtained in the assumptions and methodologies applied, and such statistics are being obtained. A challenge remains to not only make the remote sensor data available in real time (which is being done), but also provide real-time results of computed parameters such as cloud-top height, Richardson number, and cloud properties.

To more fully understand the different winter storms that can cause aircraft icing conditions, we intend to use more of the existing WPL remote sensing instruments and also to install new ones. During the first phase of winter icing storm program (WISP), which started on February 1 and ran until March 31, 1990, we observed several aircraft icing events. In addition to the remote sensors described in this study, those deployed by WISP included an additional radiometer at Elbert, Colorado, and additional RASS instruments at Platteville and Erie.

Acknowledgments

Without the special data produced by different groups inside WPL, this study would not have been possible. We thank Richard Beeler and Jack Snider for providing radiometer data, Peter May for generously sharing RASS data, and David Merritt for supplying wind data. E. R. Westwater suggested the moist adiabatic method to calculate cloud-top height and encouraged us to complete the study. Ed Russell of Computer Terrain Mapping provided the terrain map for Fig. 6, and Don Valentine did the schematic drawing. Martin Decker, Marcia Politovich, and Judith Schroeder provided many helpful comments. R. Rogers, M. Douglas, and E. R. Westwater critically read the manuscript. We have also benefitted from the detailed suggestions and critiques of several anonymous reviewers. We thank them all.

References

[1]Westwater, E. R., and Kropfli, R. A., "Remote Sensing Techniques of the Wave Propagation Laboratory for Measurement of Supercooled Liquid Water: Applications to Aircraft Icing," National Oceanic and Atmospheric Administration/Environmental Research Lab., NOAA TM ERL WPL-163, Boulder, CO, 1989.

[2]Hill, G. E., "Seedability of Orographic Clouds," *American Meteorological Society Monographics*, Vol. 21, 1986, pp. 127–137.

[3]Hogg, D. C., Guiraud, F. O., and Burton, E. B., "Simultaneous Observation of Cool Cloud Liquid by Ground-Based Microwave Radiometry and Icing of Aircraft," *Journal of Applied Meteorology*, Vol. 19, 1980, pp. 893–895.

[4]Deshler, T., Reynolds, D. W., and Huggins, A. W., "Physical Response of Winter Orographic Clouds over the Sierra Nevada to Airborne Seeding Using Dry Ice or Silver Iodide," *Journal of Applied Meteorology*, Vol. 29, 1990, pp. 288–330.

[5]Reynolds, D. W., "A Report on Winter Snowpack Augmentation," *Bulletin of the American Meteorological Society*, Vol. 69, 1988, pp. 1290–1299.

[6]Rauber, R. M., and Grant, L. O., "The Characteristics and Distribution of Cloud Water over the Mountains of Northern Colorado During Wintertime Storms. Part II: Spatial Distribution and Microphysical Characteristics," *Journal of Applied Meteorology*, Vol. 25, 1986, pp. 489–504.

[7]Politovich, M. K., and Olson, R. O., "An Evaluation of Aircraft Icing Forecasts for the Continental United States," *Preprints, Fourth International Conference on the Aviation Weather Systems*, American Meteorological Society, 1991, pp. 234–238.

[8]Hogg, D. C., Guiraud, F. O., Snider, J. B., Decker, M. T., and Westwater, E. R., "A Steerable Dual-Channel Microwave Radiometer for Measurement of Water Vapor and Liquid in the Troposphere," *Journal of Applied Meteorology*, Vol. 22, 1983, pp. 789–806.

[9]Westwater, E. R., "Ground-Based Determination of Low Altitude Temperature Profiles by Microwaves," *Monthly Weather Review*, Vol. 100, 1972, pp. 15–28.

[10]Peters, G., Timmermann, H., and Hinzpeter, H., "Temperature Sounding in the Planetary Boundary Layer by RASS—System Analysis and Results," *International Journal of Remote Sensing*, Vol. 4, 1983, pp. 49–63.

[11]May, P. T., Moran, K. P., and Strauch, R. G., "The Accuracy of RASS Temperature Measurements," *Journal of Applied Meteorology*, 1989, pp. 1329–1335.

[12]Neiman, P. J., Stankov, B. B., Shapiro, M. A., and May, P. T., "Radio Acoustic Sounding System (RASS) Observations of an Arctic Front," *Journal of Applied Meteorology*, Vol. 30, No. 6, 1990, pp. 881–892.

[13]Larsen, M. F., and Rottger, J., "VHF and UHF Doppler Radars as Tools for Synoptic Research," *Bulletin of the American Meteorological Society*, Vol. 63, 1982, pp. 906–1008.

[14]Hogg, D. C., et al., "An Automatic Profiler of the Temperature, Wind, and Humidity in the Troposphere," *Journal of Applied Meteorology*, Vol. 22, 1983, pp. 807–831.

[15]Schubert, W. H., Cox, S. K., Ciesielski, P. E., and Johnson-Pasqua, C. M., "Operation of a Ceilometer During the FIRE Marine Stratocumulus Experiment," Colorado State Univ., Atmospheric Science Paper 420, Fort Collins, CO, 1987.

[16]Strauch, R. G., Merritt, D. A., Moran, K. P., Weber, B. L., Wuertz, D. B., and May, P. T., "Wind Profilers for Support of Flight Operations," *Journal of Aircraft*, Vol. 26, 1989, pp. 1009–1015.

[17]*Ceilometer CT 12K Technical Manual*, Vaisala, Inc., Woburn, MA, 1986, pp. 1–400.

[18]Boatman, J. F., and Reinking, R. F., "Synoptic and Mesoscale Circulations and Precipitation Mechanisms in Shallow Upslope Storms Over the Western High Plains," *Monthly Weather Review*, Vol. 112, 1984, pp. 1725–1744.

[19]Reinking, R. F., and Boatman, J. F., "Upslope Precipitation Events," *Mesoscale Meteorology and Forecasting*, edited by P. S. Ray, American Meteorological Society, 1987, pp. 431–471.

[20]Rasmussen, R., and Politovich, M. K., "Winter Icing and Storms Project (WISP). Scientific Overview," June 1990; available from National Center for Atmospheric Research, 1850 Table Mesa Drive, Boulder, CO 80303.

[21]Velleman, P. F., and Hoaglin, D. C., *Applications, Basics, and Computing of Exploratory Data Analysis*, Duxbury Press, Boston, MA, 1981.

[22]Schroeder, J. A., Westwater, E. R., McMillin, L. M., and May, P. T., "Remote Temperature Sounding by Inverse Covariance Weighting of Soundings from TOVS and Ground-Based RASS and Radiometer Systems," *Preprints, IEEE International Geoscience and Remote Sensing Symposium*, 1990, pp. 1189–1191.

[23]Politovich, M. K., "Measurements of Hazardous Icing Conditions," *Preprints, Third International Conference on the Aviation Weather Systems*, American Meteorological Society, 1989, pp. 159–163.

[24]Politovich, M. K., "Aircraft Icing Caused by Large Supercooled Droplets," *Journal of Applied Meteorology*, Vol. 28, 1989, pp. 856–868.

[25]Decker, M. T., Popa Fotino, I. A., and Schroeder, J. A., "Remote Detection of Aircraft Icing Conditions Using Microwave Radiometers," National Oceanic and Atmospheric Administration/Environmental Research Labs., NOAA TM ERL WPL-137, Boulder, CO, 1986.

[26]Cox, S. K., Duda, D. P., Guinn, T. A., Johnson-Pasqua, C. M., Shubert, W. H., and Snider, J. B., "Analysis of Tethered Balloon Data from San Nicolas Island on 8 July 1987," Colorado State Univ. Atmospheric Science Paper 420, Fort Collins, CO, 1988.

[27]Flueck, J. A., and Reynolds, D. W., "A Forecast Experiment on Prediction of Cloud Conditions Suitable for Treatment in Sierra Nevada," *Preprints, 11th Conference on Weather Modification*, American Meteorological Society, 1987, pp. 13–17.

[28]Gossard, E. E., Strauch, R. G., and Rogers, R. R., "Evolution of Drop-Size Distribution in Liquid Precipitation Observed by Ground-Based Doppler Radar," *Journal of Atmospheric and Oceanic Technology*, Vol. 7, 1990, pp. 815–828.

[29]Hansman, R. J., Jr., "The Influence of Ice Accretion Physics on the Forecasting of Aircraft Icing Conditions," *Preprints, Third International Conference on the Aviation Weather System*, American Meteorological Society, 1989, pp. 154–158.

[30]Stankov, B. B., Westwater, E. R., Snider, J. B., and Weber, R. L., "Remote Measurements of Supercooled Integrated Liquid Water During WISP/FAA Aircraft Icing Program," *Journal of Aircraft*, Vol. 29, No. 4, 1992, pp. 604–611.

[31]Heggli, M. F., and Rauber, R. M., "The Characteristics and Evolution of Supercooled Water in Wintertime Storms over the Sierra Nevada: A Summary of Microwave Radiometric Measurements Taken

During the Sierra Cooperative Pilot Project," *Journal of Applied Meteorology*, Vol. 27, 1988, pp. 989–1015.

[32]Bedard, A. J., Jr., Canavero, F., and Einaudi, F., "Atmospheric Gravity Waves and Aircraft Turbulence Encounters," *Journal of the Atmospheric Sciences*, Vol. 43, 1986, pp. 2838–2844.

[33]Pobanz, B., and Marwitz, J., "Conditions Associated with Large Drop Regions," AIAA Paper 91-0353, 1991.

[34]Reuter, G. W., Wright, C. J., and Eyre, D., "Effects of Turbulence on the Growth of a Cloud Drop Spectrum," *Journal of the Atmospheric Sciences*, Vol. 46, 1989, pp. 1407–1410.

[35]Baker, M. B., Corbin, R. G., and Latham, J., "The Influence of Entrainment on the Evolution of Cloud Droplet Spectra: A Model of Inhomogeneous Mixing," *Quarterly Journal of the Royal Meteorological Society*, Vol. 106, 1980, pp. 581–598.

[36]Heggli, M. F., and Reynolds, D. W., "Radiometric Observations of Supercooled Liquid Water Within a Split Front over the Sierra Nevada," *Journal of Climate and Applied Meteorology*, Vol. 24, 1985, pp. 1258–1261.

[37]Popa Fotino, I. A. P., Schroeder, J. A., and Decker, M., "Ground-Based Detection of Aircraft Icing Conditions Using Microwave Radiometers," *IEEE Transactions on Geoscience and Remote Sensing*, Vol. GE-24, 1986, pp. 975–982.

[38]Rauber, R. M., and Grant, L. O., "Supercooled Liquid Water Structure of a Shallow Orographic Cloud System in Southern Utah," *Journal of Climate and Applied Meteorology*, Vol. 26, 1987, pp. 208–215.

[39]Sassen, K., Rauber, R. M., and Snider, J. B., "Multiple Remote Sensor Observations of Supercooled Liquid Water in a Winter Storm at Beaver, Utah," *Journal of Applied Meteorology*, Vol. 25, 1986, pp. 825–854.

[40]Caplan, S. J., Bedard, A. J., Jr., and Decker, M. T., "The 700–500 mb Lapse Rate as an Index of Microburst Probability: An Application for Thermodynamic Profilers," *Journal of Applied Meteorology*, Vol. 29, 1990, pp. 680–687.

[41]Bedard, A. J., Jr., "The Use of Remote Sensors and Laboratory Scale Models in Wake Vortex Advisory Systems," *Proceedings of the Aircraft Wake Vortices Conference* (Reno, NV), Vol. 1, AIAA, Washington, DC, 1991, pp. 50-1–50-22.